ChemPubSoc Europe

DOI: 10.1002/chem.201901617

CHEMISTRY A European Journal Full Paper

Cycloaddition |*Hot Paper*|

Dual Activation of Aromatic Diels–Alder Reactions

Ayush K. Narsaria,[a] Trevor A. Hamlin,*[a] Koop Lammertsma,*[a, b] and F. Matthias Bickelhaupt*[a, c]

Abstract: The unusually fast Diels–Alder reactions of [5]cyclophanes were analyzed by DFT at the BLYP-D3(BJ)/TZ2P level of theory. The computations were guided by an integrated activation-strain and Kohn–Sham molecular orbital analysis. It is revealed why both [5]metacyclophane and [5]paracyclophane exhibit a significant rate enhancement compared to their planar benzene analogue. The activation strain analyses revealed that the enhanced reactivity originates from 1) predistortion of the aromatic core resulting in a reduced activation strain of the aromatic diene, and/or 2) enhanced interaction with the dienophile through a distortion-controlled lowering of the HOMO–LUMO gap within the diene. Both of these physical mechanisms and thus the rate of Diels–Alder cycloaddition can be tuned through different modes of geometrical distortion (*meta* versus *para* bridging) and by heteroatom substitution in the aromatic ring. Judicious choice of the bridge and heteroatom in the aromatic core enables effective tuning of the aromatic Diels–Alder reactivity to achieve activation barriers as low as 2 kcal mol^{-1}, which is an impressive 35 kcal mol^{-1} lower than that of benzene.

Introduction

The [4+2] Diels–Alder cycloaddition of benzene is either exceptionally slow or forbidden owing to its aromatic nature.[1,2] Harsh reaction conditions, Lewis-acidic catalysts such as $AlCl_3$, or highly reactive dienophiles such as dicyanoacetylene, perfluoro-2-butyne, or tetrafluorobenzyne are required to enable reactions with benzene (Scheme 1 a).[1,2] In contrast, the strained arene-like paracyclophanes exhibit a remarkable enhancement of reactivity (see Scheme 1 b).[2] This enhanced reactivity of cyclophanes was originally proposed to arise from the localized cyclohexatriene nature of the π-conjugated core.[3] Sola and co-workers found a decrease in aromaticity in bent benzene rings compared to planar benzene by evaluating the NICS parameter.[4] Later, the enhanced reactivity was ascribed primarily to the concomitant release of strain in the transition state (TS).[5] A revealing example of the difference in reactivity between benzene and [5]metacyclophane[6] is the transfer of the carbene-like phosphinidene $PhP(CO)_4$ from a phosphanorbornadiene to the strained hydrocarbon by [4+1] cycloaddition (Scheme 1 c).[7] Removal of the transition metal group reduces the stability of the product, which then undergoes a cheletropic elimination to regenerate [5]metacyclophane.[8]

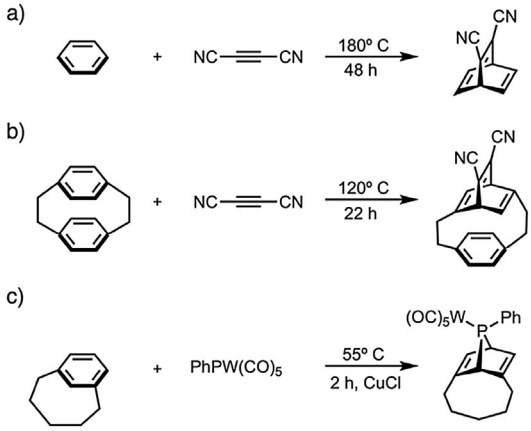

Scheme 1. Diels–Alder cycloadditions of a) benzene[2a] and b) predistorted [2.2]paracyclophane[2a] with dicyanoacetylene. c) [4+1] Cycloaddition of [5]metacyclophane and a phosphinidene complex.[7]

Early semi-empirical MNDO and Xα calculations attributed the reduced HOMO–LUMO (H–L) gap in cyclophanes to the

[a] A. K. Narsaria, Dr. T. A. Hamlin, Prof. Dr. K. Lammertsma, Prof. Dr. F. M. Bickelhaupt
Department of Theoretical Chemistry and Amsterdam Center for Multiscale Modeling (ACMM)
Vrije Universiteit Amsterdam
De Boelelaan 1083, 1081 HV Amsterdam (The Netherlands)
E-mail: t.a.hamlin@vu.nl
f.m.bickelhaupt@vu.nl

[b] Prof. Dr. K. Lammertsma
Department of Chemistry, University of Johannesburg
Auckland Park, Johannesburg, 2006 (South Africa)
E-mail: k.lammertsma@vu.nl

[c] Prof. Dr. F. M. Bickelhaupt
Institute for Molecules and Materials (IMM), Radboud University
Heyendaalseweg 135, 6525 AJ Nijmegen (The Netherlands)

Supporting information and the ORCID identification number(s) for the author(s) of this article can be found under: https://doi.org/10.1002/chem.201901617.

distortion of the π framework.[9] A recent high-level DFT analysis by Fernández and co-workers on (2,7)pyrenophanes identified reduced activation strain as the main reason for its enhanced Diels–Alder cycloaddition reactivity over that of the parent planar pyrene molecule,[10] whereas both the diminished strain in the product and the increased interaction of HOMO−1 of the arene with the LUMO of the phosphinidene were considered to be the main factors for the [4+1] cycloaddition to [5]metacyclophane.[7] Very recently, orbital interactions, and not activation strain, were proposed as the primary channel controlling the reactivity of Diels–Alder cycloadditions with strained cycloalkenes.[11] Moreover, UV/Vis measurements on [*n*]paracyclophanes indicated redshifted absorption maxima upon decrease in bridge length, which was ascribed to the decrease of the H–L gap.[12] This suggests that modulating the H–L gap of the arene by structural distortion influences its reactivity. Hence, a mechanism other than predistortion may govern the reactivity for Diels–Alder cycloaddition with bent benzene molecules. To confirm this hypothesis and to determine the factors controlling the Diels–Alder reactivity of cyclophanes, we undertook a comprehensive quantum-chemical study of the Diels–Alder cycloaddition of benzene (**B**) and its strained analogues [5]paracyclophane (**P**)[13] and [5]metacyclophane (**M**)[6] with acetylene (**A**). Acetylene was chosen as the dienophile in the investigated Diels–Alder reactions for the sake of simplicity, as it is the archetypal dienophile reactant. In line with expectation, the activation barrier for the reactions with the dicyano-substituted acetylene is about 10 kcal mol^{-1} less than for the parent acetylene and trends in reactivity are the same (Table S1 in the Supporting Information).

Theoretical Methods

Computational details

Kohn–Sham DFT calculations were performed with the ADF.2017.208 program.[14] The GGA density functional BLYP[15] with finite damping introduced by Becke and Johnson (BJ), BLYP-D3(BJ),[16] was used for the geometry optimizations of all stationary states as well as for the reaction coordinate by using the activation strain model (ASM)[17] and energy decomposition analysis (EDA).[18] As demonstrated by Grimme et al., BJ damping shows improvement over DFT-D3 in calculating barrier heights and reaction energies.[16] Specifically, BJ damping outperforms other DFT functionals in terms of more accurate treatment of the noncovalent and π–π interactions leading to both more accurate cyclophane geometries and more accurate reaction barrier heights.[16,19]

All calculations were performed with the all-electron TZ2P basis set, which is of triple-ζ quality, combined with two sets of polarization functions for all the atoms.[20] The accuracy of the integration grid (Becke grid)[21] and fit scheme (Zlm fit)[22] were set to VERY-GOOD. The energies reported herein are all for isolated molecules. Analytical frequency[23] calculations were performed to characterize the nature of the stationary points. The reactants and the cycloadducts showed real frequencies indicating their location on the potential-energy surface (PES) as local minima, while the transition state (TS) showed one imaginary frequency. The character of the eigenvector corresponding to the imaginary frequency was analyzed to ensure it was associated with the reaction under consideration. The PES of the reaction was obtained by performing intrinsic reaction coordinate (IRC) calculations.[24] All of the reported energies are electronic energies without zero-point energy correction. Furthermore, the computed reactivity trends are unchanged on considering either the Gibbs free or electronic energies (Table S8 in the Supporting Information).

Activation strain model

The activation strain model (ASM), also known as the distortion/interaction model,[25] is a fragment-based approach that essentially describes the height of the reaction barrier in terms of the reactants involved along the reaction coordinate ζ.[17] This approach has been paramount for the current understanding of different fundamental transformations in organic and organometallic chemistry.[26] In this model, the PES $\Delta E(\zeta)$ is decomposed along ζ into two energy components: the strain $\Delta E_{strain}(\zeta)$ associated with deforming the reactants from their equilibrium structures and the interaction $\Delta E_{int}(\zeta)$ between these distorted reactants along ζ. The activation barrier arises due to an intricate interplay between $\Delta E_{strain}(\zeta)$ and $\Delta E_{int}(\zeta)$ [Eq (1)].

$$\Delta E(\zeta) = \Delta E_{strain}(\zeta) + \Delta E_{int}(\zeta) \quad (1)$$

$\Delta E_{strain}(\zeta)$ is determined by the flexibility of the reactants and the extent to which they must reorganize to partake in the reaction, and $\Delta E_{int}(\zeta)$ is determined by the electronic structure and the spatial arrangement of the reactants. The strain and interaction energy terms are highly dependent on the position of the TS on the reaction coordinate ζ. Therefore, we define ζ as the projection of the intrinsic reaction coordinate onto the shorter C···C bond-forming distance, as this geometrical parameter is critically involved in the reaction and undergoes a well-defined change during the reaction.[27]

Energy decomposition analysis

$\Delta E_{int}(\zeta)$ was further analyzed in terms of quantitative molecular orbital theory as contained in Kohn–Sham DFT in combination with a canonical EDA.[18] The EDA decomposes $\Delta E_{int}(\zeta)$ into the following physically meaningful energy terms [Eq. (2)]:

$$\Delta E_{int}(\zeta) = \Delta V_{elstat}(\zeta) + \Delta E_{Pauli}(\zeta) + \Delta E_{oi}(\zeta) + \Delta E_{disp}(\zeta) \quad (2)$$

Therein, $\Delta V_{elstat}(\zeta)$ represents the quasiclassical electrostatic interactions between the unperturbed charge distributions of the distorted reactants. The Pauli repulsion $\Delta E_{Pauli}(\zeta)$ emerges due to repulsive exchange interactions between the occupied closed-shell orbitals. The orbital interactions $\Delta E_{oi}(\zeta)$ comprise stabilizing interactions such as electron-pair bonding, charge transfer between occupied and unoccupied molecular orbitals, and polarization (empty–occupied orbital mixing on one fragment due to the presence of another fragment). Lastly, $\Delta E_{disp}(\zeta)$ accounts for the dispersion forces originating from noncovalent interactions or weak interactions.

Results and Discussion

The optimized geometries of the ground-state reactants are shown in Figure 1. The cyclophanes are formed by the addition of a short five-membered oligomethylene bridge to benzene (**B**) at the *para* and *meta* positions. The oligomethylene bridge induces several geometrical distortions in the cyclophanes. The most prominent is the out-of-plane bending of the aromatic core (α and γ) into a symmetrical [5]paracyclophane (**P**) and an

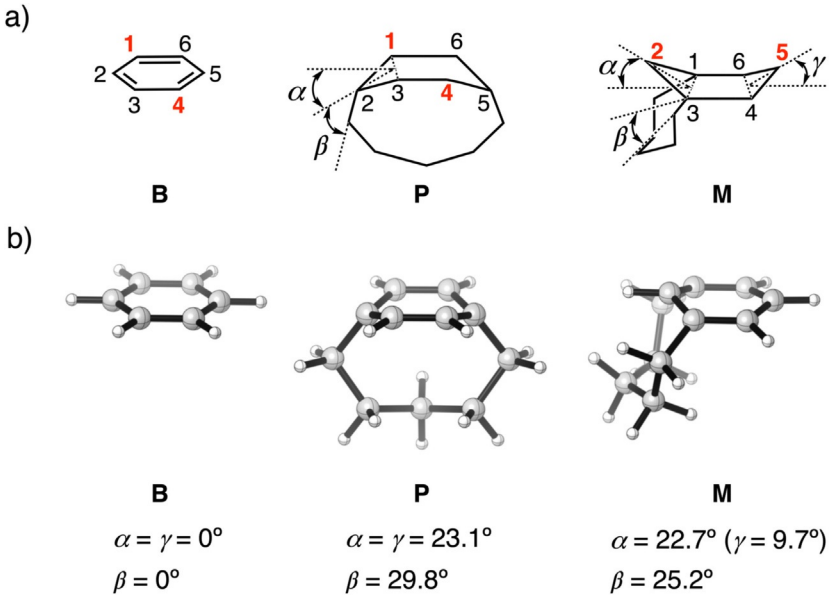

Figure 1. a) Illustration with atom numbering, where red bold numbers indicate the bond-forming C atoms that react with acetylene, and structural parameters: out-of-plane bending of the aromatic core (α and γ) and bending of the bridge with respect to the core (β). The C=C double bonds in the aromatic core of **P** and **M** have been omitted for clarity. b) Ground-state equilibrium geometries of the dienes, computed at the BLYP-D3(BJ)/TZ2P level of theory.

asymmetrical [5]metacyclophane (**M**) boat-like configurations (Figure 1 a). Additionally, there is distortion in the benzylic carbon–carbon bonds of the bridge relative to the aromatic core, depicted as β.

We began by analyzing the Diels–Alder reactivity of **B**, **P**, and **M** with **A**. The reactions of **B** and **P** proceed via concerted synchronous transition states, whereas that of **M** is concerted asynchronous (Figure 2). The Diels–Alder cycloaddition reactions of the cyclophanes proceed earlier compared to benzene. The late transition state in **B** is associated with the highest activation energy (37.2 kcal mol^{-1}), while the earlier TSs for cyclophanes **P** (23.6 kcal mol^{-1}) and **M** (16.7 kcal mol^{-1}) are associated with markedly lower barriers, which is consistent with the Hammond–Leffler postulate.[28] The activation energy is reduced by up to about 20 kcal mol^{-1} and the total reaction energy ΔE_{rxn} changes from being endothermic (6.9 kcal mol^{-1}) to highly exothermic (ca. −28 kcal mol^{-1}) when moving from **B** to the cyclophanes.

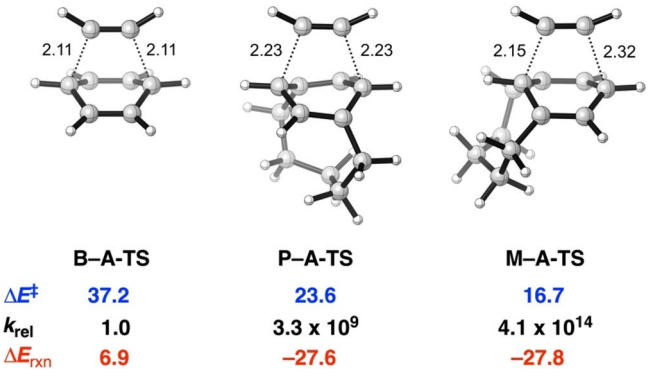

Figure 2. Transition state structures with forming bond lengths [Å], computed activation energy barrier $\Delta E^{\ddagger}$ [kcal mol^{-1}] (blue), relative rate constants k_{rel} (black), and total reaction energies ΔE_{rxn} [kcal mol^{-1}] (red) for the Diels–Alder cycloaddition reactions of **B**, **P**, and **M** with **A**, computed at the BLYP-D3(BJ)/TZ2P level of theory.

The physical factors governing the reactivity of **B**, **P**, and **M** toward **A** were analyzed quantitatively by means of ASM and EDA and are represented graphically in Figure 3. Figure 3 b reveals that the enhanced Diels–Alder cycloaddition reactivity for **M** results from a significant decrease in strain energy ΔE_{strain}, whereas ΔE_{int} is comparable to **B**. Decomposing ΔE_{strain} into the strain-energy components of the two reactants (**M** and **A**) $\Delta E_{strain(diene)}$ and $\Delta E_{strain(dienophile)}$ reveals that the much lower strain originates largely from the reduced strain contribution of **M** (Figure 3 c). The reason for this behavior is that the cyclophane bridge connecting the *meta* positions (i.e., C1 and C3, see Figure 1 a for atom numbering) pulls the two sides of the aromatic core (i.e., C1–C6 and C3–C4) towards each other. As a consequence, the bond-forming carbon centers C2 and C5 are forced out of the aromatic plane into a boat conformation and thereby facilitate formation of new C–C bonds with the incoming **A**. Hence, the equilibrium geometry of **M** resembles more the TS geometry than that of **B**, which is not subject to such predistortion. The aromatic core of **P** is, of course, also predistorted, but unlike that of **M** not with respect to the bond-forming carbon centers (i.e., C1 and C4), resulting in a ΔE_{strain} similar to that of **B**.

To quantify the contribution of strain towards the Diels–Alder barrier heights of **B**, **P**, and **M**, we analyzed the energy terms at a consistent TS-like geometry, because the magnitude of the strain and the interaction energy terms is highly dependent on the position of the TS on the reaction coordinate.[16,27] Therefore, to ensure an equitable comparison of energies, we analyzed the geometries in which the shorter of the two C···C bond-forming lengths is 2.15 Å. Hereafter, this position on the

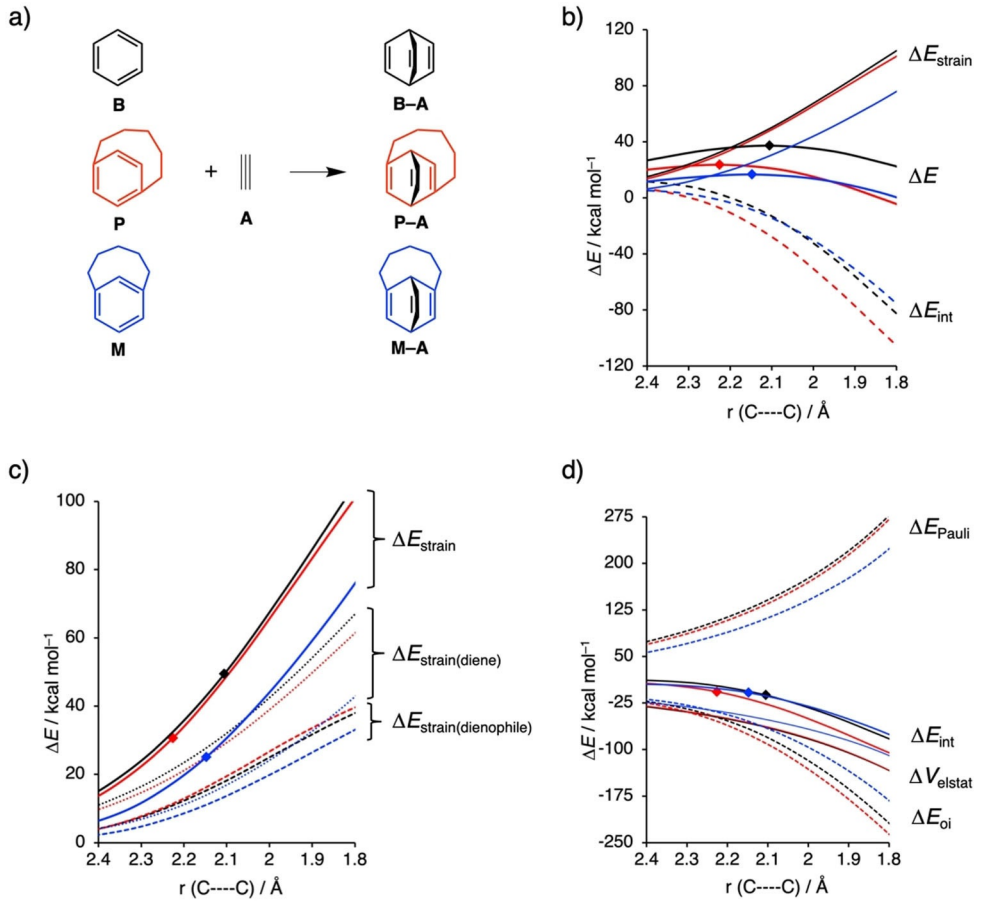

Figure 3. a) Model reactions of **A** with **B** (black), **P** (red), and **M** (blue). b) Activation strain analyses, c) strain decomposition, and d) energy decomposition analyses of the Diels–Alder cycloaddition reactions, computed at the BLYP-D3(BJ)/TZ2P level of theory (TS position marked by diamonds) and projected onto the shorter of the two C···C bond-forming lengths [Å]. Analyses of the complete reaction path are provided in Figure S1 in the Supporting Information.

Table 1. Activation strain analysis [kcal mol^{-1}] computed at ζ^* by using BLYP-D3(BJ)/TZ2P.

Compd	ΔE^*	ΔE^*_{int}	ΔE^*_{strain}	$\Delta E^*_{strain(diene)}$	$\Delta E^*_{strain(dienophile)}$
B	36.3	−6.9	43.2	27.9	15.3
P	21.9	−19.8	41.7	25.4	16.3
M	16.6	−8.2	24.8	13.8	11.0

reaction coordinate is denoted as ζ^* and the corresponding energy terms as ΔE^*. The structures and energies at ζ^* are similar to the actual TSs and the trend in energies mirrors the trend at the real TS (see Figure 2 and Table 1).

Smaller changes in α and γ over the course of the Diels–Alder reaction result in less-destabilizing $\Delta E_{strain(diene)}$. Figure 4 shows that in order to react with **A**, **M** must be distorted least from its equilibrium geometry ($\Delta\alpha = 17^\circ$ and $\Delta\gamma = 19^\circ$), then **P** ($\Delta\alpha = \Delta\gamma = 22^\circ$), and then finally **B** ($\Delta\alpha = \Delta\gamma = 31^\circ$). Therefore, at ζ^*, the $\Delta E^*_{strain(diene)}$ value of **M** is 14.1 kcal mol^{-1}, which is about 11.6 kcal mol^{-1} lower than those of both **B** and **P** (see Table 1). As already noted, the geometry of **M** shows the smallest change due to its favorable predistortion. The substantially lower ΔE^*_{strain} of **M** compared to **B** and **P** also originates from the lower $\Delta E^*_{strain(dienophile)}$ at ζ^* (Table 1). This effect was traced to the relatively small distortion of **A** in the Diels–Alder cycloaddition, which is related to the asynchronous nature of its TS. The asynchronicity stems from the interaction of the two nonidentical (different local environments) carbon atoms C2 and C5 in **M**, which causes the new C–C bonds to form at different rates. This behavior is evident from the different C2-C1-H and C1-C2-H bond angles of **A** in the ζ^* of **M**–**A** (see Figure 4a for atom numbering) of 153 and 160°, respectively. These distortions are, however, much larger ($\approx$150°) for **B**–**A** and **P**–**A** compared to the linear acetylene equilibrium geometry. Previously, it was concluded that concomitant release of strain in the diene drives the Diels–Alder cycloaddition reaction of **M**,[29] but instead it appears that its enhanced reactivity results from a reduced buildup of strain along the reaction coordinate in both the diene and dienophile.

The enhanced reactivity of *para*-bridged **P** compared to **B** originates from the difference in their stabilizing ΔE_{int} component (Figure 3b). EDA analysis shows that this arises mainly from the different contributions of the orbital interaction term ($\Delta\Delta E_{oi} = 9$ kcal mol^{-1}; Figure 3d; Table S2 in the Supporting Information). A comprehensive Kohn–Sham molecular orbital (KS-MO) analysis[18] revealed that the more stabilizing ΔE^*_{oi} for **P** arises primarily from a stronger inverse electron-demand interaction from $HOMO_A$ to $LUMO_P$ (Figure 5). The **P**–**A** donor–ac-

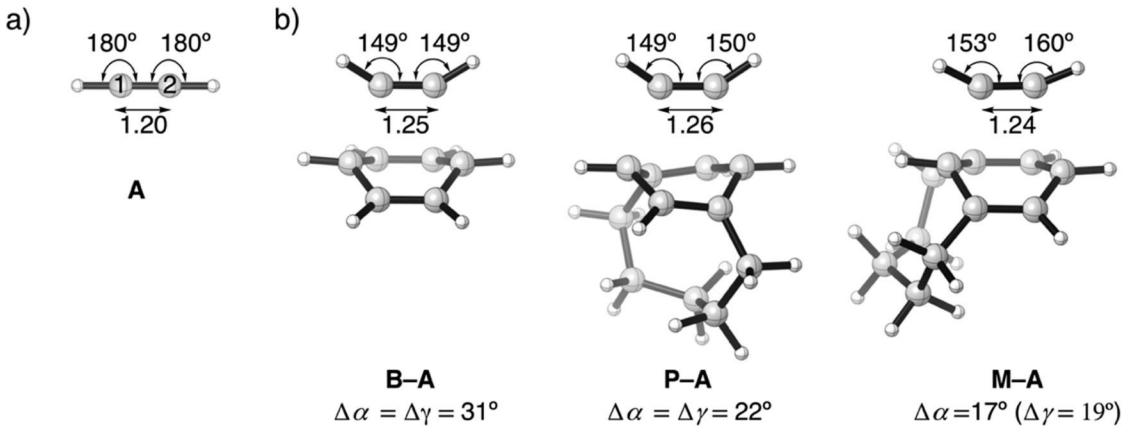

Figure 4. a) Equilibrium structure of **A** with the atom numbering (bond lengths in Å) and b) structures of **B**–**A**, **P**–**A** and **M**–**A** showing the change in structural parameters (bond lengths in Å), computed at ζ* by using BLYP-D3(BJ)/TZ2P.

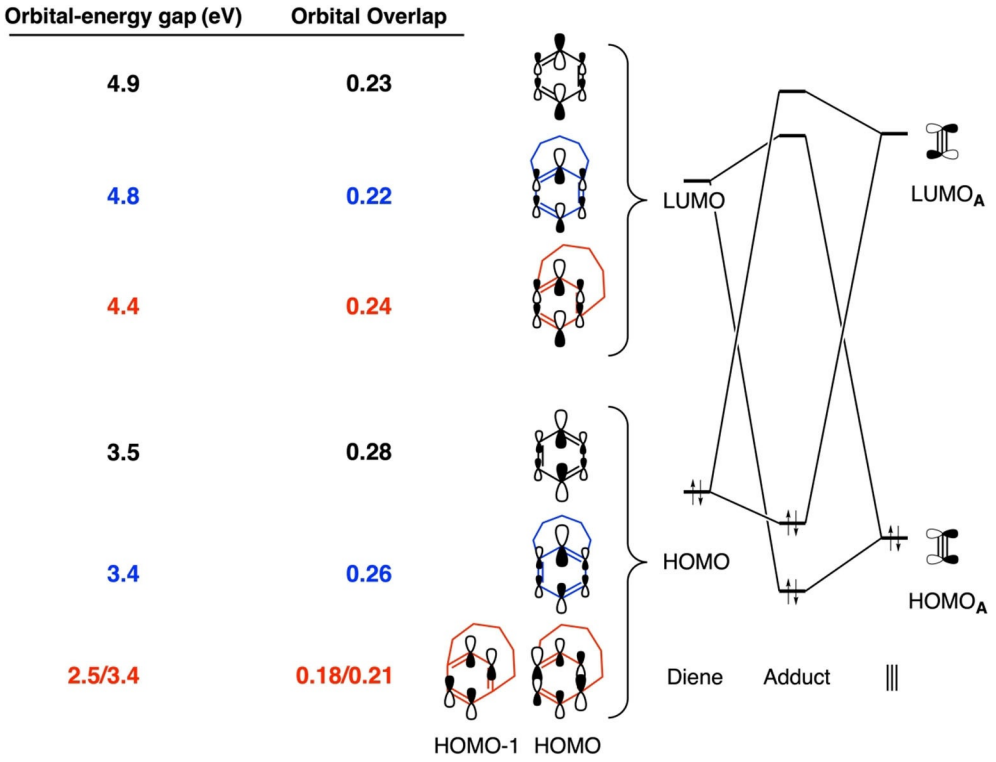

Figure 5. Schematic MO interaction diagram based on quantitative KS-MO analyses of normal and inverse electron-demand orbital-energy gap and overlap in the Diels–Alder cycloaddition reactions of **A** with **B** (black), **P** (red), and **M** (blue), computed at ζ* by using BLYP-D3(BJ)/TZ2P. The illustrated MOs are representative of the electronic structure of the reactants at ζ*.

ceptor orbital-energy gap of 4.4 eV and bond overlap of 0.24 are more favorable for **P** than for **B** (orbital-energy gap = 4.9 eV, $S = 0.23$). Importantly, both normal and inverse orbital interactions are more stabilizing for **P** than for **B** due to smaller orbital-energy gaps, but the former contributes to a lesser degree due to poor $HOMO_P/HOMO-1_P$ bond overlap (both orbitals participate in a normal electron-demand interaction) with $LUMO_A$. The poor overlap results from a small amplitude of the occupied frontier orbitals at the bond-forming carbon centers (see Figure 5). Thus, both normal and inverse electron-demand orbital interaction in **P**–**A** is driven by the decrease in orbital-energy gaps.

Of the three Diels–Alder cycloadditions, the orbital-energy gap is the smallest and thus most favorable along the **P**–**A** reaction coordinate (Figure 6). The origin of this behavior is the smaller H–L gap within the diene **P** (3.2 eV at its equilibrium geometry) compared to that within **B** (5.0 eV at its equilibrium geometry). Such a small H–L gap is caused by structural distortion imparted by the short *para* bridge, which manifests itself in a large out-of-plane bending of the aromatic core ($\alpha \approx 23^\circ$)

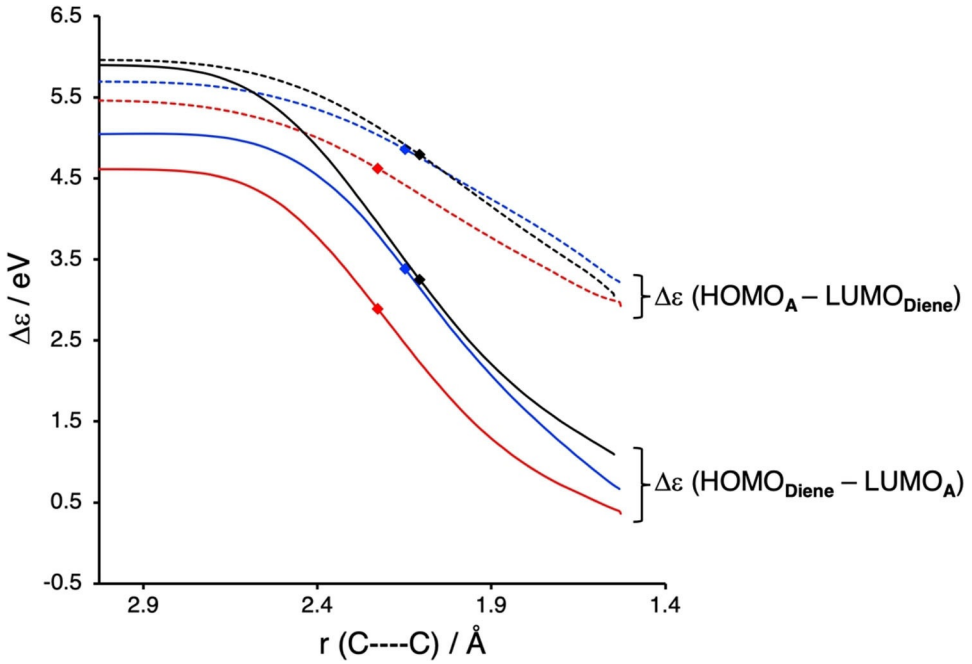

Figure 6. Orbital-energy gap analysis along the reaction coordinate (black: **B**–**A**, red: **P**–**A**, blue: **M**–**A**), computed at the BLYP-D3(BJ)/TZ2P level of theory. Diamonds represent the position of the TS.

and the related bending of the bridge ($\beta \approx 30^\circ$) at the equilibrium geometry. To understand how these geometrical distortions contribute to a markedly lower H–L gap, we performed a comprehensive quantitative KS-MO analysis.

Out-of-plane distortion α of the planar aromatic core causes the destabilization and stabilization of π-HOMO and π*-LUMO, respectively (Figure 7a and Figure S2 in the Supporting Information). The antibonding π-HOMO is destabilized due to an increase in π–π overlap $S_{\pi\text{-}\pi}$ between the p_π amplitudes of the

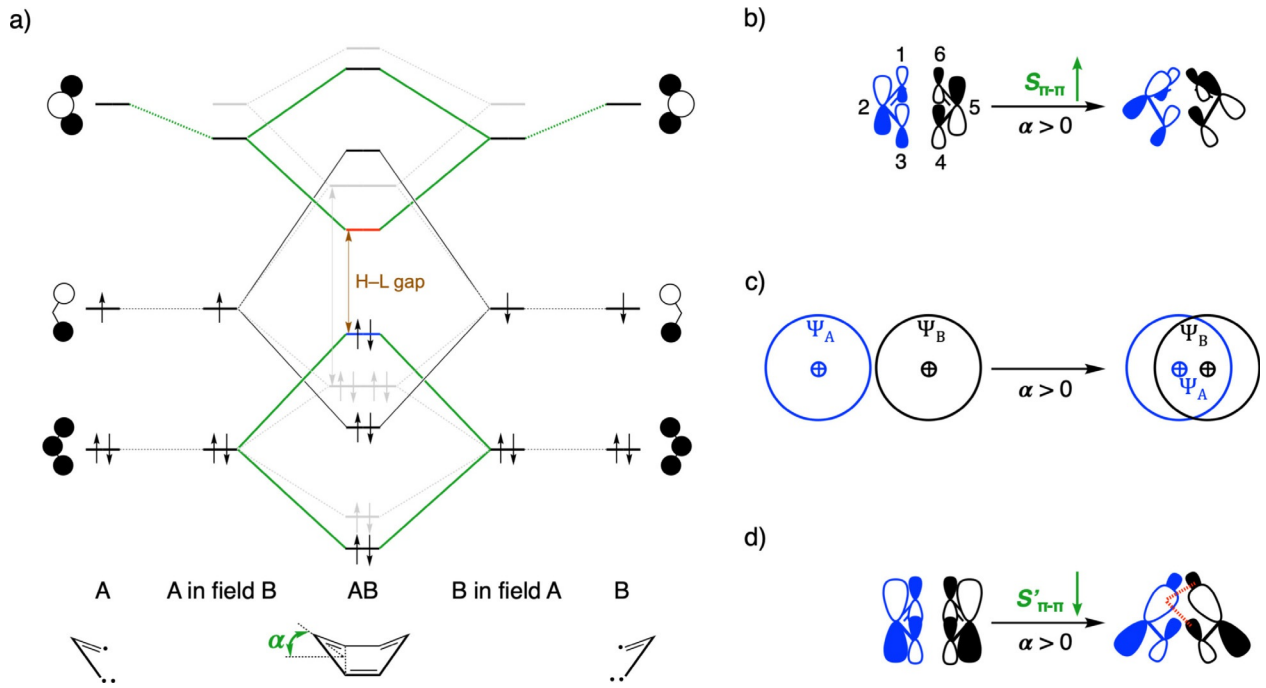

Figure 7. a) Schematic π-fragment-orbital interaction diagram between two equivalent allylic fragments depicting the lowering of H–L gap upon out-of-plane distortion (α) relative to flat benzene (in gray). The factors that change the H–L gap are b) the increase in overlap ($S_{\pi\text{-}\pi}$) between allylic π-HOMOs, c) the electrostatic stabilization of the allylic π*-LUMOs (ψ_A and ψ_B denote the π*-LUMOs belonging to fragments A and B, respectively), and d) the decrease in overlap ($S'_{\pi-\pi}$) between allylic π*-LUMOs with the red dotted lines indicating out-of-phase overlap between the diffuse p_π orbitals.

π-HOMO fragment orbitals of the equivalent allylic C_3H_3 triradical fragments forming the overall benzene molecule (Figure 7b and Table S3 in the Supporting Information). The π*-LUMO is stabilized due to the attractive Coulombic (electrostatic) interaction stemming from the increase in overlap of the π*-LUMO fragment orbital of one allylic C_3H_3 triradical fragment with the nuclei of the other and vice versa (Figure 7c).[18] This overlap increases as the spatial proximity between the allylic fragments decreases. As a result, the isolated allylic π*-LUMO is stabilized, which in turn stabilizes the overall bonding π*-LUMO of benzene (see Figure 7a and Figure S2 in the Supporting Information, quantitative details are provided in Table S4 in the Supporting Information). Contrary to intuition, there is a decrease in π*–π* overlap $S'_{\pi-\pi}$ upon bending (Table S3 in the Supporting Information). This is caused by the cancellation of overlap on out-of-phase mixing of the diffuse p_π amplitude of the π* LUMO on the terminal C atom of one fragment and the front C atom of the other (Figure 7d). Thus, the H–L energy gap within **B** decreases upon out-of-plane distortion by 1) increased π–π overlap that destabilizes the HOMO, and 2) enhanced electrostatic stabilization that stabilizes the LUMO despite an unanticipated reduction in π*+π* overlap. Furthermore, an increase in the bending of the benzylic C–C bond β (see Figure 1a) results in mixing of the σ and π fragment orbitals of the ring substituents and the aromatic core, respectively, which thereby enhances both the destabilization of the antibonding π-HOMO and the stabilization of the bonding π* LUMO and thus contributes to decreasing the H–L gap even further (Figure 8 and Figure S3 in the Supporting Information). The outlined relationship between structural distortion (geometrical strain) and the H–L gap sheds new light on the findings of Hopf and co-workers, who attributed the enhanced reactivity of [*n*]paracyclophanes over **B** solely to the sterically strained geometries.[30]

Thus, structural distortion reduces the H–L energy gap within **P** and accelerates its Diels–Alder cycloaddition because of the enhanced **P**–**A** orbital interaction, as reflected in ΔE_{oi} (red curves in Figure 6). Cyclophane **M** exhibits a smaller **M**–**A** orbital-energy gap than the parent system **B**–**A** at the start of the cycloaddition (blue and black curve, respectively, in Figure 6). However, the orbital-energy gaps become similar around the TS, despite the fact that the H–L gap within **M** is decreased relative to that within **B** (4.0 eV in **M** versus 5.0 eV in **B** at equilibrium geometry) due to a similar mechanism as discussed for **P**. Note that although HOMO−1 of **M** interacts with $LUMO_A$ in the early stages of the reaction, HOMO and HOMO−1 of **M** being nearly degenerate ($\Delta\varepsilon = 0.30$ eV) invert near the TS due to the change in electronic structure caused by increased out-of-plane distortion along the reaction coordinate (see Figure S4 in the Supporting Information). The reason for the similar orbital-energy gap around the TS comes from a larger H–L energy gap within the dienophile **A**, as its distortion is much smaller around the TS (Figure 4b) on reacting with **M** than it is for both **B** or **P**. In other words, the initial relatively small **M**–**A** orbital-energy gap increases around the TS due to the smaller C-C-H bending of **A**, which translates into a higher π-HOMO and a lower π*-LUMO energy.[31] The fact that the bending of **A** is relatively small is related to the asynchronous nature of the TS in **M**–**A**, as already discussed above. The outcome is a larger normal and inverse electron-demand orbital-energy gap and consequently a less stabilizing ΔE^*_{oi} for **M**–**A**, which amounts to only −54 as opposed to −78 and −68 kcal mol^{-1} for **P**–**A** and **B**–**A**, respectively (Table S2 in the Supporting Information).

Next, we assessed whether, besides structural distortion, the $(CH_2)_5$ bridge of the cyclophane also exerts an electronic influence on the reactivity, but found the effect on reaction barrier heights to be minimal. For example, removing the bridge from **M** (**M**-**nb**) and **P** (**P**-**nb**) leads to negligible changes in ΔE^*_{int}. Removing the distortion in the aromatic core and simulating the electronic effect of the bridge by using *meta*- and *para*-xylene led to activation barrier heights that are almost comparable to that of **B**. It then appears that predistortion of the aromatic core by the bridge enhances the Diels–Alder cycloaddition reactivity and not the substituent effect itself (see Figure S5 and Table S6 in the Supporting Information).

To apply these insights for the design of aromatic Diels–Alder reactions with significantly lower activation energy barriers, we combined the two modes of activation induced by geometrical distortion: reduced activation strain of the diene connected by a *meta* bridge and enhanced orbital interactions through a reduced H–L gap within the diene connected by a *para* bridge. The latter can also be addressed through means other than distortion, such as heteroatom substitution in the aromatic core. Heteroatom-substituted benzene derivatives of main group elements show interesting electronic properties, such as a smaller H–L gap,[32] as well as an enhanced cycloaddition reactivity.[33] For example, in contrast to benzene, both substituted phosphabenzene[34] and substituted azadiene[35] have been shown to react with mild dienophiles, albeit sluggishly, indicating a still relatively high activation barrier. Therefore, as proof-of-concept, we systematically designed and explored the behavior of the aromatic Diels–Alder cycloaddition for four heteroatom-functionalized [5]metacyclophanes: The C4 atom of **M** is substituted for one heteroatom (see Figure 1a for atom numbering) in $\mathbf{M_{(N)}}$ (pyridine core) and $\mathbf{M_{(P)}}$ (phospha-

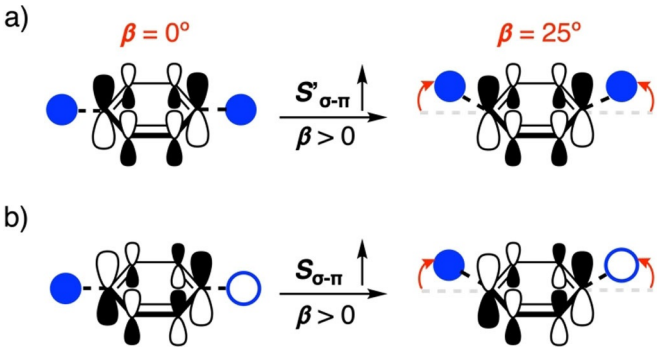

Figure 8. Schematic overview of the effect of bending of substituted aromatic carbon atoms (angle β in red) on the a) in-phase ($S'_{\sigma-\pi}$, π*-LUMO) and; (b) out-of-phase ($S_{\sigma-\pi}$, π-HOMO) overlap of the σ and π fragment orbitals of the substituent and the aromatic core, respectively. For clarity, the $-(CH_2)_5$ bridge of **P** is represented in a simplified manner as two H atoms (blue).

benzene core); the C4 and C6 atoms of **M** are substituted for two heteroatoms in $\mathbf{M}_{(2N)}$ (pyrimidine core) and $\mathbf{M}_{(2P)}$ (diphosphabenzene core). We envisioned that introducing a heteroatom into the aromatic core of the favorably predistorted [5]metacyclophane would cause a further reduction in the H–L gap within **M** (see Table S7 in the Supporting Information) and result in an enhanced stabilizing orbital interaction with the dienophile in tandem with a reduced activation strain. Figure 9

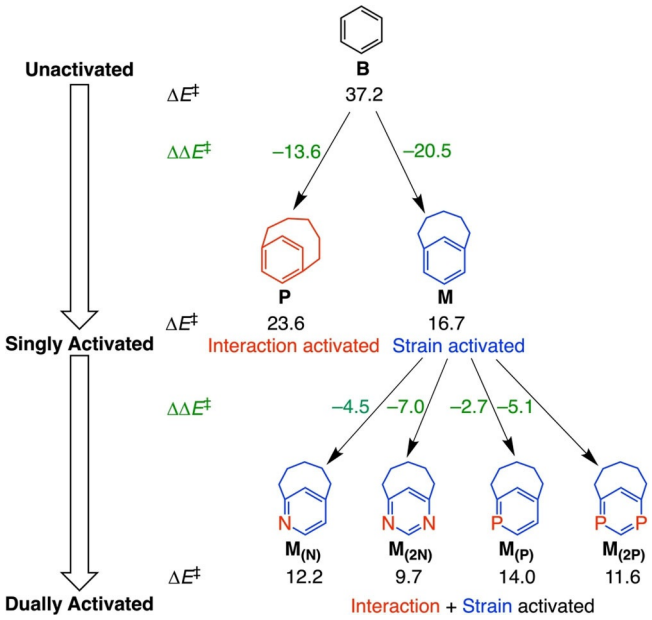

Figure 9. Combining the modes of activation for aromatic Diels–Alder cycloadditions at the carbon centers starting from the archetypal **B**. Activation energies $\Delta E^{\ddagger}$ in black, changes in the activation energy barrier $\Delta\Delta E^{\ddagger}$ introduced by an additional mode of activation in green, computed at the BLYP-D3(BJ)/TZ2P level of theory. All energies are in kcal mol^{-1}.

summarizes the progressive decrease in activation barrier on successive introduction of strain and/or interaction activation through geometrical distortion and subsequent heteroatom substitution in the aromatic core. As anticipated, the computed activation barriers decrease sharply from single activation, that is, from bending of benzene to the [5]metacyclophane, to dual activation, that is, from carbonaceous [5]metacyclophane to heteroatom-functionalized [5]metacyclophane. The barrier height decreases along the series $\mathbf{M}_{(P)} > \mathbf{M}_{(N)} > \mathbf{M}_{(2P)} > \mathbf{M}_{(2N)}$ (Table S8 in the Supporting Information). The pyrimidine containing $\mathbf{M}_{(2N)}$ has the lowest cycloaddition activation barrier of this series of only 9.7 kcal mol^{-1}, which is 27.5 kcal mol^{-1} lower than for **B** and 7.0 kcal mol^{-1} lower than that of its parent **M** (see Table S8 in the Supporting Information). The steady decrease in barrier height for these heteroatom-functionalized [5]metacyclophanes, as predicted, arises mostly from an enhanced interaction energy that results from more stabilizing orbital interactions compared to **M**.

The orbital interactions for $\mathbf{M}_{(2P)}$ are more stabilizing than for $\mathbf{M}_{(P)}$ due to a lower π*-LUMO energy (see Table S7 in the Supporting Information) resulting in a smaller $\mathbf{M}_{(2P)}$–**A** orbital-energy gap and thus a lower barrier. The nitrogen-substituted metacyclophanes, $\mathbf{M}_{(N)}$ and $\mathbf{M}_{(2N)}$, both show enhanced interaction compared to [5]metacyclophane, coming mostly from an increase in orbital interactions in the former and a decrease in Pauli repulsion in the latter, along with a reduced activation strain in both cases (Figures S6 and S7 in the Supporting Information). These factors are fully consistent with the findings of earlier studies.[35c,d] The difference in cycloaddition barrier between the reactive nitrogen- and the relatively less reactive phosphorus-substituted metacyclophanes arises from a higher destabilizing activation strain in the latter compared to the former (Figures S6–S9 in the Supporting Information).

To expand the scope of the work, we also analyzed the Diels–Alder reactivity of heteroatom-substituted metacyclophanes in which one C–C and one C–X bond (X = N, P substituted at the C2 center of **M**, see Figure 1a for atom numbering) are formed (see Scheme 2). Formation of a C–N bond

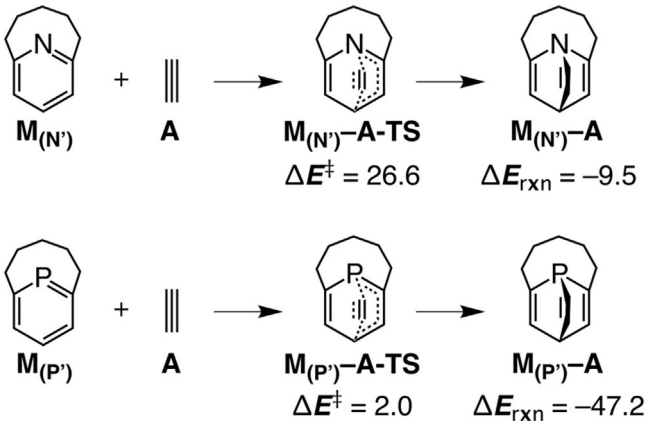

Scheme 2. Aromatic Diels–Alder cycloadditions of $\mathbf{M}_{(N')}$ and $\mathbf{M}_{(P')}$, which involve formation of a C–X bond (X = N, P). Activation energies $\Delta E^{\ddagger}$ and reaction energy ΔE_{rxn} in kcal mol^{-1}.

during a cycloaddition has a higher activation barrier than formation of the corresponding C–C bond.[35d,36] We observed this expected trend in barrier height for the cycloaddition of $\mathbf{M}_{(N')}$, which is associated with a much higher activation barrier ($\Delta E^{\ddagger} = 26.6$ kcal mol^{-1}, see Scheme 2) than **M** due to a higher Pauli repulsion combined with a destabilizing activation strain (see Figure S10 in the Supporting Information). However, a remarkable enhancement of cycloaddition reactivity is observed for the reaction involving C–P bond formation in $\mathbf{M}_{(P')}$, which has the lowest activation barrier ($\Delta E^{\ddagger} = 2.0$ kcal mol^{-1}, see Scheme 2) among all the studied reactions due to greatly enhanced interaction energy. The latter results from a significantly stabilizing orbital interaction, which overcompensates the destabilizing activation strain, compared to **M** (Figure S11 in the Supporting Information). A KS-MO analysis at consistent geometry ζ* revealed significantly small $\mathbf{M}_{(P')}$–**A** orbital-energy gaps corresponding to normal (1.6 eV) and inverse (3.6 eV) electron-demand interaction compared to its parent **M**. A phosphorus atom, substituted at the C2 or C5 center (C2 in our case) of **M**, acts as both an auxiliary donor (destabilizing the π-HOMO of **M**) and an acceptor (stabilizing the π*-LUMO

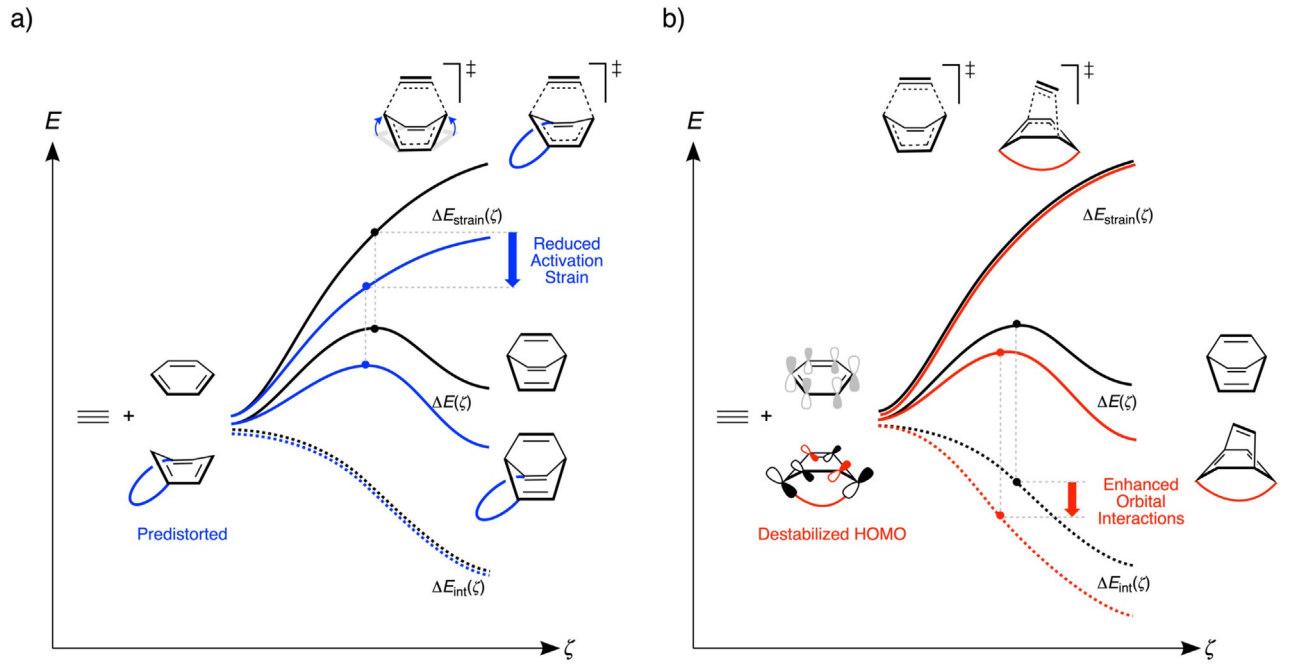

Scheme 3. Activation strain diagram of the Diels–Alder cycloadditions of a) **A** with **B** (in black) and **M** (in blue; reduced activation strain); and b) **A** with **B** (in black) and **P** (in red; enhanced orbital interaction). The five-membered oligomethylene bridge is depicted schematically in blue for **M** and in red for **P**. Only the most important contribution to the distinct activations is illustrated.

of **M**)[32] and results in the smallest H–L gap within $\mathbf{M}_{(P')}$ of 2.5 eV at equilibrium geometry (see Table S7 in the Supporting Information), compared to the other dienes in our study. Moreover, the orbital overlap of the key orbitals participating in inverse electron-demand interaction, $HOMO_A$ and $LUMO_{M(P')}$, is more favorable ($S = 0.30$) compared to **M** or even **P** ($S = 0.22$ and 0.24 for **M** and **P**, respectively). This increase in overlap stems from a large amplitude of the $\mathbf{M}_{(P')}$ π^*-LUMO on the bond-forming phosphorus center due to the low-lying empty p_π orbital of phosphorus. In this way we rationally tune the aromatic Diels–Alder cycloaddition rate of benzene to cover a wide spectrum of activation barriers through simple manipulation of different activation channels (see Scheme 3).

Conclusion

The acceleration of aromatic Diels–Alder reactions through structural distortion of the aromatic core, for example, in cyclophanes, consists of two distinct physical mechanisms: 1) a decrease in activation strain, as well as 2) an enhanced TS interaction, as follows from our quantum chemical activation–strain analyses. These two mechanisms may contribute to different extents for clearly identifiable reasons. Thus, the Diels–Alder barrier of aromatic dienes reacting with acetylene, for example, decreases from 37 to 24 to 17 kcal mol^{-1} along the series benzene, [5]paracyclophane, and [5]metacyclophane. While the reduced barrier in both cyclophanes is induced by structural distortion of the aromatic core, the reduced barrier in the reaction of [5]paracyclophane mainly stems from a more stabilizing TS interaction with the dienophile, whereas the further reduced barrier for [5]metacyclophane is primarily caused by lowering of the activation strain due to a favorable predistortion (see Scheme 3).

The short five-membered bridge of [5]metacyclophane pulls the two *meta* carbon atoms of the aromatic core together, and this causes the bond-forming carbon atoms to point out of the aromatic plane and towards the dienophile. This predistorted aromatic core closely resembles the TS geometry and leads to a reduced activation strain. The bridge in [5]paracyclophane, on the other hand, pulls the two *para* carbon atoms towards each other, whereas the bond-forming carbon atoms are left unaffected and as such not favorably predistorted, which is associated with a significantly smaller reduction in activation strain. Instead, [5]paracyclophane reacts more rapidly compared to benzene, due to the more stabilizing orbital interactions that arise from a distortion-induced decrease of the H–L gap within the diene. The latter is chiefly the result of the out-of-plane bending of the aromatic core induced by the oligomethylene bridge, which has, among others, the effect of destabilizing the π-HOMO due to an increase in antibonding p_π–p_π overlap. Similar to [5]paracyclophane, the H–L gap also decreases within [5]metacyclophane, but this decrease is offset by an increase in the H–L gap within acetylene leading to larger donor–acceptor orbital-energy gaps, and thus less stabilizing orbital interactions, compared to the reaction of [5]paracyclophane.

Interestingly, the distortion-driven mechanisms discussed above can now also be addressed individually through different means. A reduced activation strain can be directly leveraged by employing a *meta*-connected cyclophane bridge. On the other hand, stronger interaction, originating from a much smaller H–L gap in [5]paracyclophane, can also be induced

through, for example, main-group heteroatom substitution in [5]metacyclophane. As a proof-of-concept, the dually activated (reduced activation strain plus stronger interaction) $\mathbf{M}_{(P')}$ featuring C–P bond formation in a *meta*-bridged phosphabenzene has an aromatic Diels–Alder barrier of only 2 kcal mol^{-1}, which is almost 35 kcal mol^{-1} lower than that of benzene. In this way, we highlight the ability to tune aromatic Diels–Alder cycloadditions by means of multiple activation channels. We envisage that this might also be utilized for the activation of small molecules.

Acknowledgements

This work is part of the Industrial Partnership Program (IPP) "Computational Sciences for Energy Research" (project 14CSER011), which is part of the Netherlands Organization for Scientific Research (NWO). This research program is co-financed by Shell Global Solutions International B.V. Additionally, we thank The Netherlands Organization for Scientific Research (NWO) for financial support.

Conflict of interest

The authors declare no conflict of interest.

Keywords: activation strain model · arenes · cycloaddition · cyclophanes · density functional calculations

[1] a) J. Sauer, *Angew. Chem. Int. Ed. Engl.* **1967**, *6*, 16 – 33; *Angew. Chem.* **1967**, *79*, 76 – 94; and references cited therein; b) R. S. H. Liu, C. G. Krespan, *J. Org. Chem.* **1969**, *34*, 1271 – 1278; c) J. P. N. Brewer, H. Heaney, *Tetrahedron Lett.* **1965**, *6*, 4709 – 4712; d) G. Zhong, B. Chan, L. Radom, *J. Am. Chem. Soc.* **2007**, *129*, 924 – 933; e) J. J. Torres-Vega, A. Vásquez-Espinal, L. Ruiz, M. A. Fernández-Herrera, L. Alvarez-Thon, G. Merino, W. Tiznado, *ChemistryOpen* **2015**, *4*, 302 – 307.

[2] a) E. Ciganek, *Tetrahedron Lett.* **1967**, *8*, 3321 – 3325; b) D. J. Cram, H. Steinberg, *J. Am. Chem. Soc.* **1951**, *73*, 5691 – 5704; c) C. J. Brown, A. C. Farthing, *Nature* **1949**, *164*, 915 – 916; d) D. J. Cram, J. M. Cram, *Acc. Chem. Res.* **1971**, *4*, 204 – 213.

[3] a) F. Bickelhaupt, W. H. de Wolf, *Recl. Trav. Chim. Pays-Bas* **2010**, *107*, 459 – 478; b) F. Bickelhaupt, W. H. de Wolf, *Adv. Strain Org. Chem.* **1993**, *3*, 185 – 227.

[4] F. Feixas, E. Matito, J. Poater, M. Solà, *J. Phys. Chem. A* **2007**, *111*, 4513 – 4521.

[5] a) G. W. Wijsman, W. M. Boesveld, M. C. Beekman, M. S. Goedheijt, B. L. M. van Baar, F. J. J. de Kanter, W. H. de Wolf, F. Bickelhaupt, *Eur. J. Org. Chem.* **2002**, *4*, 614 – 629; b) P. A. Kraakman, J. M. Valk, H. A. G. Niederlander, D. B. E. Brouwer, F. M. Bickelhaupt, W. H. De Wolf, F. Bickelhaupt, C. H. Stam, *J. Am. Chem. Soc.* **1990**, *112*, 6638 – 6646; c) L. W. Jenneskens, H. J. R. De Boer, W. H. De Wolf, F. Bickelhaupt, *J. Am. Chem. Soc.* **1990**, *112*, 8941 – 8949.

[6] a) J. W. van Straten, W. H. de Wolf, F. Bickelhaupt, *Tetrahedron Lett.* **1977**, *18*, 4667 – 4670; b) L. A. M. Turkenburg, W. H. de Wolf, F. Bickelhaupt, *Tetrahedron Lett.* **1983**, *24*, 1817 – 1820.

[7] M. J. van Eis, C. M. D. Komen, F. J. J. de Kanter, W. H. de Wolf, K. Lammertsma, F. Bickelhaupt, M. Lutz, A. L. Spek, *Angew. Chem. Int. Ed.* **1998**, *37*, 1547 – 1550; *Angew. Chem.* **1998**, *110*, 1656 – 1658.

[8] M. J. van Eis, H. Zappey, F. J. J. de Kanter, W. H. de Wolf, K. Lammertsma, F. Bickelhaupt, *J. Am. Chem. Soc.* **2000**, *122*, 3386 – 3390.

[9] a) L. W. Jenneskens, F. J. J. de Kanter, W. H. de Wolf, F. Bickelhaupt, *J. Comput. Chem.* **1987**, *8*, 1154 – 1169; b) L. W. Jenneskens, J. N. Louwen, W. H. De Wolf, F. Bickelhaupt, *J. Phys. Org. Chem.* **1990**, *3*, 295 – 300; c) R. B. Remington, T. J. Lee, H. F. Schaefer, *Chem. Phys. Lett.* **1986**, *124*, 199 – 201.

[10] Y. García-Rodeja, I. Fernández, *J. Org. Chem.* **2017**, *82*, 8157 – 8164.

[11] a) B. J. Levandowski, T. A. Hamlin, F. M. Bickelhaupt, K. N. Houk, *J. Org. Chem.* **2017**, *82*, 8668 – 8675; b) B. J. Levandowski, T. A. Hamlin, R. C. Helgeson, F. M. Bickelhaupt, K. N. Houk, *J. Org. Chem.* **2018**, *83*, 3164 – 3170.

[12] a) D. J. Cram, C. S. Montgomery, G. R. Knox, *J. Am. Chem. Soc.* **1966**, *88*, 515 – 525; b) A. D. Wolf, V. V. Kane, R. H. Levin, M. Jones, *J. Am. Chem. Soc.* **1973**, *95*, 1680 – 1680; c) N. L. Allinger, J. T. Sprague, T. Liljefors, *J. Am. Chem. Soc.* **1974**, *96*, 5100 – 5104; d) V. V. Kane, A. D. Wolf, M. Jones, *J. Am. Chem. Soc.* **1974**, *96*, 2643 – 2644; e) P. Rademacher, in *Modern Cyclophane Chemistry* (Eds.: R. Gleiter, H. Hopf), Wiley-VCH, Weinheim, **2004**, pp. 275 – 310.

[13] a) L. W. Jenneskens, F. J. J. De Kanter, P. A. Kraakman, L. A. M. Turkenburg, W. E. Koolhaas, W. H. De Wolf, F. Bickelhaupt, Y. Tobe, K. Kakiuchi, Y. Odaira, *J. Am. Chem. Soc.* **1985**, *107*, 3716 – 3717; b) J. E. Rice, T. J. Lee, R. B. Remington, W. D. Allen, D. A. Clabo, H. F. Schaefer, *J. Am. Chem. Soc.* **1987**, *109*, 2902 – 2909.

[14] a) G. te Velde, F. M. Bickelhaupt, E. J. Baerends, C. Fonseca Guerra, S. J. A. van Gisbergen, J. G. Snijders, T. Ziegler, *J. Comput. Chem.* **2001**, *22*, 931 – 967; b) C. Fonseca Guerra, J. G. Snijders, G. te Velde, E. J. Baerends, *Theor. Chem. Acc.* **1998**, *99*, 391 – 403; c) ADF2017, SCM Theoretical Chemistry; Vrije Universiteit: Amsterdam, The Netherlands, **2017**; http://www.scm.com.

[15] a) A. D. Becke, *Phys. Rev. A* **1988**, *38*, 3098 – 3100; b) C. Lee, W. Yang, R. G. Parr, *Phys. Rev. B* **1988**, *37*, 785 – 789; c) B. G. Johnson, P. M. W. Gill, J. A. Pople, *J. Chem. Phys.* **1993**, *98*, 5612 – 5626; d) T. V. Russo, R. L. Martin, P. J. Hay, *J. Chem. Phys.* **1994**, *101*, 7729 – 7737.

[16] a) S. Grimme, J. Antony, S. Ehrlich, H. Krieg, *J. Chem. Phys.* **2010**, *132*, 154104; b) S. Grimme, S. Ehrlich, L. Goerigk, *J. Comput. Chem.* **2011**, *32*, 1456 – 1465; c) T. A. Hamlin, D. Svatunek, S. Yu, L. Ridder, I. Infante, L. Visscher, F. M. Bickelhaupt, *Eur. J. Org. Chem.* **2019**, 378 – 386.

[17] a) F. M. Bickelhaupt, K. N. Houk, *Angew. Chem. Int. Ed.* **2017**, *56*, 10070 – 10086; *Angew. Chem.* **2017**, *129*, 10204 – 10221; b) I. Fernández, F. M. Bickelhaupt, *Chem. Soc. Rev.* **2014**, *43*, 4953 – 4967; c) F. M. Bickelhaupt, *J. Comput. Chem.* **1999**, *20*, 114 – 128; d) M. Contreras, E. Osorio, F. Ferraro, G. Puga, K. J. Donald, J. G. Harrison, G. Merino, W. Tiznado, *Chem. Eur. J.* **2013**, *19*, 2305 – 2310.

[18] a) F. M. Bickelhaupt, E. J. Baerends, in *Reviews in Computational Chemistry* (Eds.: K. B. Lipkowitz, D. B. Boyd), John Wiley & Sons, Hoboken, **2000**, pp. 1 – 86; b) R. van Meer, O. V. Gritsenko, E. J. Baerends, *J. Chem. Theory Comput.* **2014**, *10*, 4432 – 4441.

[19] A. Karton, L. Goerigk, *J. Comput. Chem.* **2015**, *36*, 622 – 632.

[20] E. van Lenthe, E. J. Baerends, *J. Comput. Chem.* **2003**, *24*, 1142 – 1156.

[21] M. Franchini, P. H. T. Philipsen, L. Visscher, *J. Comput. Chem.* **2013**, *34*, 1819 – 1827.

[22] M. Franchini, P. H. T. Philipsen, E. van Lenthe, L. Visscher, *J. Chem. Theory Comput.* **2014**, *10*, 1994 – 2004.

[23] a) A. Bérces, R. M. Dickson, L. Fan, H. Jacobsen, D. Swerhone, T. Ziegler, *Comput. Phys. Commun.* **1997**, *100*, 247 – 262; b) H. Jacobsen, A. Bérces, D. P. Swerhone, T. Ziegler, *Comput. Phys. Commun.* **1997**, *100*, 263 – 276.

[24] a) L. Deng, T. Ziegler, L. Fan, *J. Chem. Phys.* **1993**, *99*, 3823 – 3835; b) L. Deng, T. Ziegler, *Int. J. Quantum Chem.* **1994**, *52*, 731 – 765.

[25] a) D. H. Ess, K. N. Houk, *J. Am. Chem. Soc.* **2008**, *130*, 10187 – 10198; b) D. H. Ess, K. N. Houk, *J. Am. Chem. Soc.* **2007**, *129*, 10646 – 10647.

[26] a) T. A. Hamlin, M. Swart, F. M. Bickelhaupt, *ChemPhysChem* **2018**, *19*, 1315 – 1330; b) T. A. Hamlin, B. van Beek, L. P. Wolters, F. M. Bickelhaupt, *Chem. Eur. J.* **2018**, *24*, 5927 – 5938; c) M. A. van Bochove, G. Roos, C. Fonseca Guerra, T. A. Hamlin, F. M. Bickelhaupt, *Chem. Commun.* **2018**, *54*, 3448 – 3451; d) S. Yu, H. M. de Bruijn, D. Svatunek, T. A. Hamlin, F. M. Bickelhaupt, *ChemistryOpen* **2018**, *7*, 995 – 1004; e) P. Vermeeren, X. Sun, F. M. Bickelhaupt, *Sci. Rep.* **2018**, *8*, 10729; f) X. Sun, M. V. J. Rocha, T. A. Hamlin, J. Poater, F. M. Bickelhaupt, *Phys. Chem. Chem. Phys.* **2019**, *21*, 9651 – 9664.

[27] a) W.-J. van Zeist, A. H. Koers, L. P. Wolters, F. M. Bickelhaupt, *J. Chem. Theory Comput.* **2008**, *4*, 920 – 928.

[28] a) J. E. Leffler, *Science* **1953**, *117*, 340 – 340; b) G. S. J. Hammond, *J. Am. Chem. Soc.* **1955**, *77*, 334 – 338.

[29] a) L. A. M. Turkenburg, P. M. L. Blok, W. H. de Wolf, F. Bickelhaupt, *Angew. Chem. Int. Ed. Engl.* **1982**, *21*, 298 – 301; *Angew. Chem.* **1982**, *94*, 291 –

292; b) F. Bickelhaupt, W. H. de Wolf, *J. Phys. Org. Chem.* **1998**, *11*, 362 – 376.

[30] K.-L. Noble, H. Hopf, M. Jones, S. L. Kammula, *Angew. Chem. Int. Ed. Engl.* **1978**, *17*, 602 – 602; *Angew. Chem.* **1978**, *90*, 629 – 630.

[31] T. A. Hamlin, B. J. Levandowski, A. K. Narsaria, K. N. Houk, F. M. Bickelhaupt, *Chem. Eur. J.* **2019**, *25*, 6342 – 6348.

[32] A. K. Narsaria, J. Poater, C. Fonseca Guerra, A. W. Ehlers, K. Lammertsma, F. M. Bickelhaupt, *J. Comput. Chem.* **2018**, *39*, 2690 – 2696.

[33] a) S. Yruegas, J. H. Barnard, K. Al-Furaiji, J. L. Dutton, D. J. D. Wilson, C. D. Martin, *Organometallics* **2018**, *37*, 1515 – 1518; b) D. Wu, R. Ganguly, Y. Li, S. N. Hoo, H. Hirao, R. Kinjo, *Chem. Sci.* **2015**, *6*, 7150 – 7155; c) D. Wu, L. Kong, Y. Li, R. Ganguly, R. Kinjo, *Nat. Commun.* **2015**, *6*, 7340; d) T. Chu, G. I. Nikonov, *Chem. Rev.* **2018**, *118*, 3608 – 3680, and references within; e) T. Ishii, K. Suzuki, T. Nakamura, M. Yamashita, *J. Am. Chem. Soc.* **2016**, *138*, 12787 – 12790.

[34] a) G. Märkl, F. Lieb, *Angew. Chem. Int. Ed. Engl.* **1968**, *7*, 733 – 733; *Angew. Chem.* **1968**, *80*, 702 – 702; b) A. J. Ashe, M. D. Gordon, *J. Am. Chem. Soc.* **1972**, *94*, 7596 – 7597.

[35] a) D. L. Boger, *Chem. Rev.* **1986**, *86*, 781 – 793; b) P. M. Graham, D. A. Delafuente, W. Liu, W. H. Myers, M. Sabat, W. D. Harman, *J. Am. Chem. Soc.* **2005**, *127*, 10568 – 10572; c) A. Talbot, D. Devarajan, S. J. Gustafson, I. Fernández, F. M. Bickelhaupt, D. H. Ess, *J. Org. Chem.* **2015**, *80*, 548 – 558; d) Y.-F. Yang, Y. Liang, F. Liu, K. N. Houk, *J. Am. Chem. Soc.* **2016**, *138*, 1660 – 1667; e) A. E. Hayden, K. N. Houk, *J. Am. Chem. Soc.* **2009**, *131*, 4084 – 4089.

[36] a) I. Fleming, *Frontier Orbitals and Organic Chemical Reactions*, Wiley, London, **1976**; b) H.-O. Ho, W.-K. Li, *J. Mol. Struct.* **2005**, *723*, 195 – 204; c) Z.-X. Yu, Q. Dang, Y.-D. Wu, *J. Org. Chem.* **2005**, *70*, 998 – 1005.

Manuscript received: April 8, 2019
Revised manuscript received: May 20, 2019
Accepted manuscript online: May 21, 2019
Version of record online: July 8, 2019

